



HAL
open science

Coupled hydrogeochemical modelling using KIRMAT to assess water-rock interaction in a saline aquifer in central-eastern Tunisia

Soumaia M’Nassri, Yann Lucas, Gerhard Schafer, Lotfi Dridi, Rajouene Majdoub

► To cite this version:

Soumaia M’Nassri, Yann Lucas, Gerhard Schafer, Lotfi Dridi, Rajouene Majdoub. Coupled hydrogeochemical modelling using KIRMAT to assess water-rock interaction in a saline aquifer in central-eastern Tunisia. *Applied Geochemistry*, 2019, 102, pp.229-242. 10.1016/j.apgeochem.2019.01.018 . hal-02981334

HAL Id: hal-02981334

<https://hal.science/hal-02981334>

Submitted on 22 Oct 2021

HAL is a multi-disciplinary open access archive for the deposit and dissemination of scientific research documents, whether they are published or not. The documents may come from teaching and research institutions in France or abroad, or from public or private research centers.

L’archive ouverte pluridisciplinaire **HAL**, est destinée au dépôt et à la diffusion de documents scientifiques de niveau recherche, publiés ou non, émanant des établissements d’enseignement et de recherche français ou étrangers, des laboratoires publics ou privés.



Distributed under a Creative Commons Attribution - NonCommercial 4.0 International License

1 **Coupled hydrogeochemical modelling using KIRMAT to assess water-rock** 2 **interaction in a saline aquifer in central-eastern Tunisia**

3 Soumaia M’Nassri^a, Yann Lucas^b, Gerhard Schäfer^{b*}, Lotfi Dridi^a, Rajouene
4 Majdoub^a

5 *^aDépartement du Génie des Systèmes Horticoles et du Milieu Naturel, Université de Sousse,*
6 *Institut Supérieur Agronomique de Chott Meriem, Sousse, Tunisia*

7 *^bUniversité de Strasbourg, CNRS, LHyGeS UMR 7517, Strasbourg, France*

8 *Corresponding author: schafer@unistra.fr
9

10 **Abstract**

11 To quantify water-rock interactions and forecast their spatiotemporal evolution in the shallow
12 aquifer of Sidi El Hani located in central-eastern Tunisia, the numerical code KIRMAT was
13 used. Based on available geological, mineralogical, thermodynamic, kinetic and
14 hydrodynamic data, the model was built and calibrated on two transects of the aquifer
15 oriented along the flow lines of groundwater. The numerical results show that the interactions
16 between water and rock are responsible for groundwater salinity, which is strongly dominated
17 by chlorides, sodium and sulphates. The variations of dissolved species in space and time are
18 the result of halite dissolution, anhydrite and gypsum dissolution and precipitation, calcite
19 dissolution and dolomite precipitation. The precipitation of dolomite can locally induce a
20 reduction in permeability and further enhance an increase in leaching because the residence
21 time between rock and water will be amplified. Three numerical sensitivity studies have been
22 conducted to evaluate the influence of water-rock interactions on groundwater salinization.
23 The study highlights the finding that the modelled fate of dissolved species in the unconfined
24 aquifer is rather sensitive to the Darcy velocity but not very sensitive to the initial volume
25 fractions of minerals in the two transects and the composition of groundwater injected at the
26 upstream boundary.

27 **Keywords:** groundwater salinization, rock-water interaction, reactive mass transport, Sidi El
28 Hani aquifer, numerical model

29 **1. Introduction**

30 In arid and semi-arid climate regions, groundwater represents the primary source of water for
31 agricultural, industrial and domestic uses (Li et al., 2013). Unfortunately, since the last few

1 decades, these resources have been affected by salinization problems, which occur in many
2 aquifers around the world (De Montaty et al., 2008; Kumar et al., 2013), as well as in the
3 Mediterranean areas (Farid et al., 2015; Eissa et al., 2016). In these regions, the reasons for
4 the degradation of the groundwater quality are mainly seawater intrusion, climate change,
5 irrigation return flow, uncontrolled fertilizer applications, dissolution of evaporites and
6 upwelling of saline waters from deep layers (Milnes, 2011; Bel Hadj Salem et al., 2012; Li et
7 al., 2014; Giambastiani et al., 2014; Han et al., 2014; Najib et al., 2016). The interaction of
8 these processes can lead to a varied composition of dissolved species in the aquifer.
9 Therefore, eliminating processes that alter groundwater quality is crucial for powerful water
10 management and protection and necessary to ensure the sustainability of precious
11 groundwater resources in arid regions (Sikdar et al., 2001; Moran-Ramírez et al., 2016).

12 In recent years, a strong effort has been undertaken to thoroughly develop hydrogeochemical
13 tools to assess groundwater quality, such as statistical and geostatistical approaches (Alberto
14 et al., 2001; Belkhiri et al., 2010), the empirical measurement of major chemical indicators,
15 the design of hydrogeochemical diagrams (Edmunds et al., 2003; Andre et al., 2005) and
16 water analysis based on isotopic techniques (Bouchaou et al., 2008). These tools provide a
17 better understanding of the interference of physical and chemical processes that affect water
18 chemistry and the residence time of the major dissolved species involved in the system.
19 However, each approach has its own limitations due to the multiplicity of geochemical
20 processes between the different phases, which adds complexity to the analysis. Additionally,
21 the mass fluxes in the aquifer and the chemical composition of the rock may strongly vary in
22 time and space (Xiao et al., 2012; Peikam and Jalali, 2015). One way to overcome these
23 problems is the use of numerical reactive transport models (Beaucaire et al., 2008; Lucas et
24 al., 2010; Montcoudiol et al., 2015; Jing et al., 2016; Nasri et al., 2016).

25 The modelling approach is an effective tool to study and predict the degradation of
26 groundwater quality (Lopez-Chicano et al., 2001; André et al., 2005; Nilde et al., 2008; Li et
27 al., 2010). In the past, a large number of geochemical programmes have been developed.
28 Among these, some of them attempt to determine the final thermodynamic equilibrium of the
29 geochemical system (Helgeson, 1968), while others take into account the phase mole transfer
30 throughout kinetic reactions (Beig and Lüttge, 2006; Burch et al., 1993). Such models are
31 useful because they provide a thorough understanding of the aquifer system. However, their
32 use remains somewhat limited for modelling mineral diagenesis coupled with dynamic
33 processes of mass transport (Nourtier-Mazauric et al., 2005; Nourtier-Mazauric, 2006).

1 Therefore, more advanced numerical tools need to be implemented for reactive transport
2 models (Gérard, 1996; Guo et al., 1997; Eary et al., 2002; Li et al., 2002; Lakshmanan et al.,
3 2003; Appelo et al., 2008; Belkhiri et al., 2010; Steefel et al., 2015; Laabidi and Bouhlila,
4 2016). They may be used to quantify the geochemical processes and predict possible changes
5 in the composition of both water and rock and the fate of dissolved species in the aquifer.

6 Therefore, advanced quantitative studies using numerical hydrogeochemical models are
7 needed to understand and study the horizontal extent of the saturated zone that may be
8 influenced by geologic alteration.

9 This paper aims to quantify the main processes of salinization of the groundwater in the basin
10 of Sidi El Hani. A coupled hydrogeochemical model was used to study and predict the
11 chemical changes that occur as water evolves along a flow path. Therefore, we used the
12 multi-component reactive transport code KIRMAT (Kinetic Reaction and Mass Transport)
13 (Gérard et al., 1996, 1998) that combines geochemical reactions and 1D mass transport
14 equations.

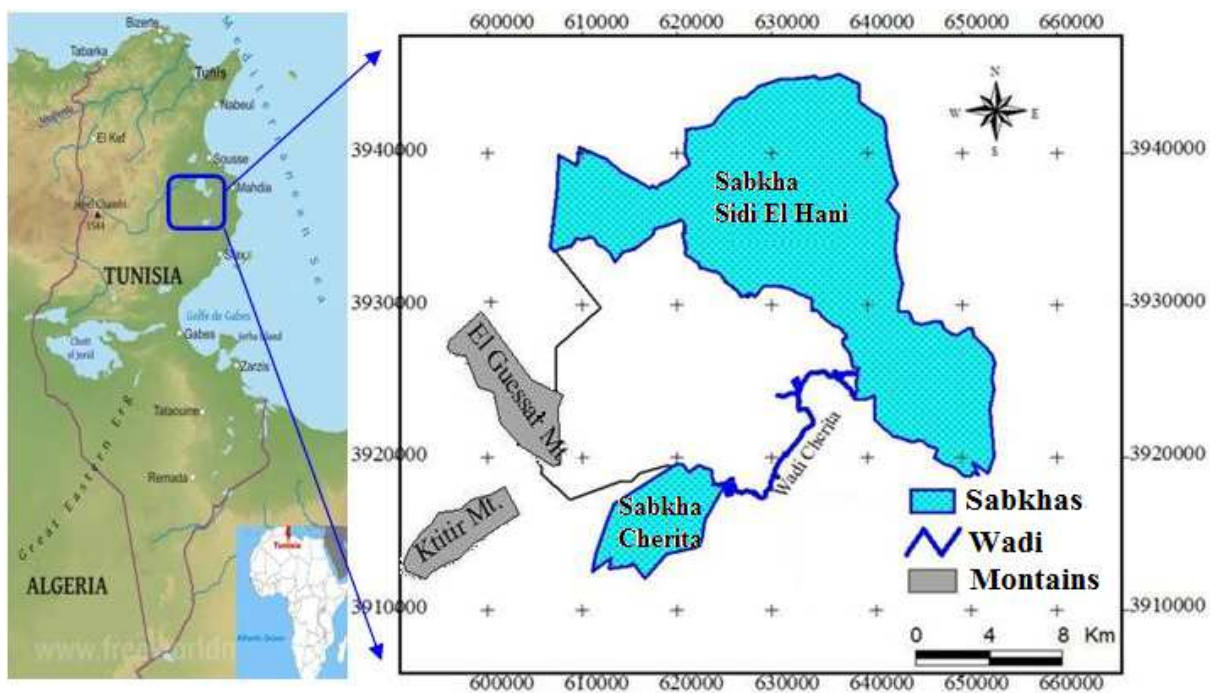
15 The main objectives are to characterize and identify the possible geochemical processes
16 acting in the groundwater and to predict the evolution of the chemical composition. To meet
17 these objectives, a multi-component reactive transport model KIRMAT was applied in this
18 study. The Sidi El Hani aquifer, where the salinity exceeds 6 g.L^{-1} to reach 8 g.L^{-1} , is
19 therefore a very suitable site to evaluate the influence of geochemical process on groundwater
20 salinization. In the first step, the response of the numerical model is evaluated by the root-
21 mean-square-error (RMSE) between the computed and observed concentrations of each
22 monitoring point. Second, once the numerical model is calibrated, a sensitivity analysis is
23 performed to identify the model input parameters that may have an influence on the reactive
24 mass transport in the aquifer. This allows us to understand and interpret the numerical results
25 of the hydrochemical model. The sensitivity study is conducted for three specific cases: i)
26 variation of the volume fraction of halite; ii) variation of the chemical composition of
27 incoming water and (iii) variation of the Darcy velocity.

28

29 **2. Material and methods**

30 *2.1. Study area, geological and hydrogeological setting*

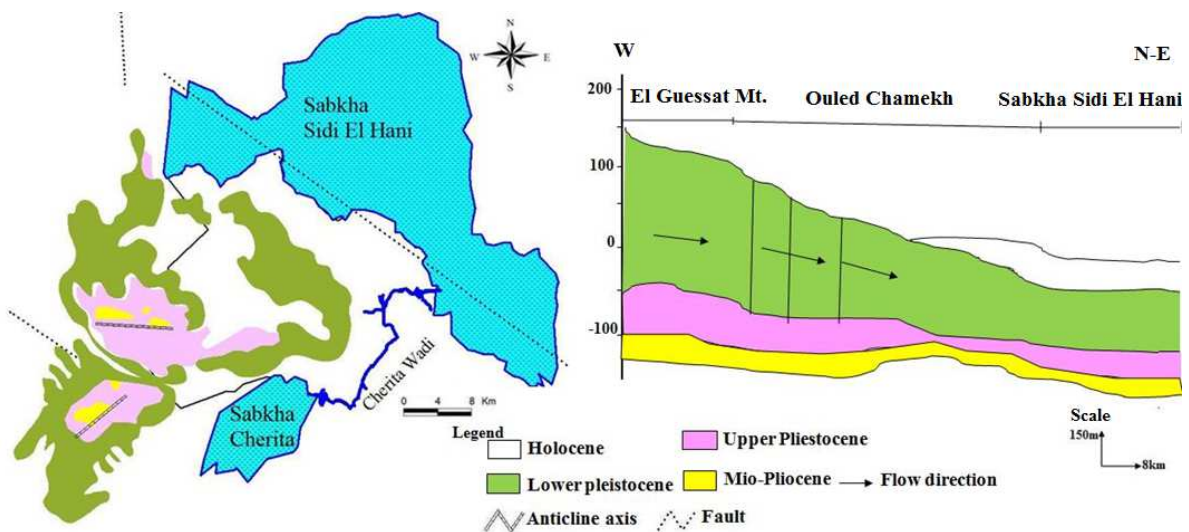
1 The investigated area is located in the centre-eastern part of Tunisia, between 35°21'-
 2 35°35'N and 10°10'-10°25'E, covering approximately 346 km². This area extends between
 3 the mountain chains of El Guezzaf and Ktitir, which barely reach more than 100 m of altitude
 4 in the western part, and the lowlands of a continental sabkha named the Sidi El Hani in the
 5 eastern and Cherita in the southern regions. The largest and permanent hydrological network
 6 in this region is Wadi Chertia, which runs from Sabkha Cherita to Sabkha Sidi El Hani (Fig.
 7 1). The plain lies within a continental arid to semi-arid climate region. The annual average
 8 rainfall is below 270 mm. The monthly average temperature varies between 9°C and 30°C in
 9 January and August, respectively. The evapotranspiration is estimated to be 1500 mm per
 10 year. As in many arid and semi-arid regions of the world, the surface waters are scarce. The
 11 aquifer is considered to be one of the main water resources of the agricultural region. The
 12 plain has been intensively cultivated for the last decade, and 75% of the area is occupied by
 13 trees, crops and cereals (Majdoub et al., 2012). However, the groundwater is no longer
 14 suitable for agricultural uses because the total concentration of dissolved salts (chlorides,
 15 sodium, sulphates) generally exceeds the limits values for irrigation water (M'nassri et al.,
 16 2016).



17
 18 **Figure 1:** Location map of the study area.

19 The Ouled Chamekh plain is Mio-Plio-Quaternary in age, comprising the Holocene (Qh), the
 20 Pleistocene (Qp) and the Mio-Pleistocene (Qmp) (Fig. 2). The Holocene formation is largely
 21 present in the study area as clays, sands, silts and evaporites (Tagorti et al., 2013). It

1 represents the superficial layer. The Pleistocene deposits can be divided into three layers. The
 2 first layer is generally below 35 m and is composed of sand, halite and carbonate deposits.
 3 The second layer is limestone and is between 35 and 45 m thick. The third layer is hard
 4 limestone, soft white limestone and silts and is 45 to 50 m thick. The Mio-Pleistocene is
 5 composed of sand with an interlayered 50 m-thick limestone. In addition, the study area lies
 6 within a collapsed zone with a synclinal form and cuttings of saline depressions along NW-
 7 SE orientations (Essefi et al., 2014). Furthermore, the Ouled Chamekh plain is sliced by a
 8 fault network that controls the Mio-Plio-Quaternary deposition, including the Ktitir, Hajeb
 9 Layoun and Sidi El Hani faults. These faults are inherited from the Cenozoic and Mesozoic
 10 formations (Ghribi, 2010; Essefi et al., 2013). The Sidi El Hani fault causes subsidence of the
 11 Sabkha Sidi El Hani along the eastern boundary of the study area. According to the
 12 mineralogical composition, the study area has quartz (60-70%), carbonate minerals and
 13 evaporites (15-20%) and clay (5-10%). The clays are mainly composed of kaolinite, illite and
 14 muscovite.

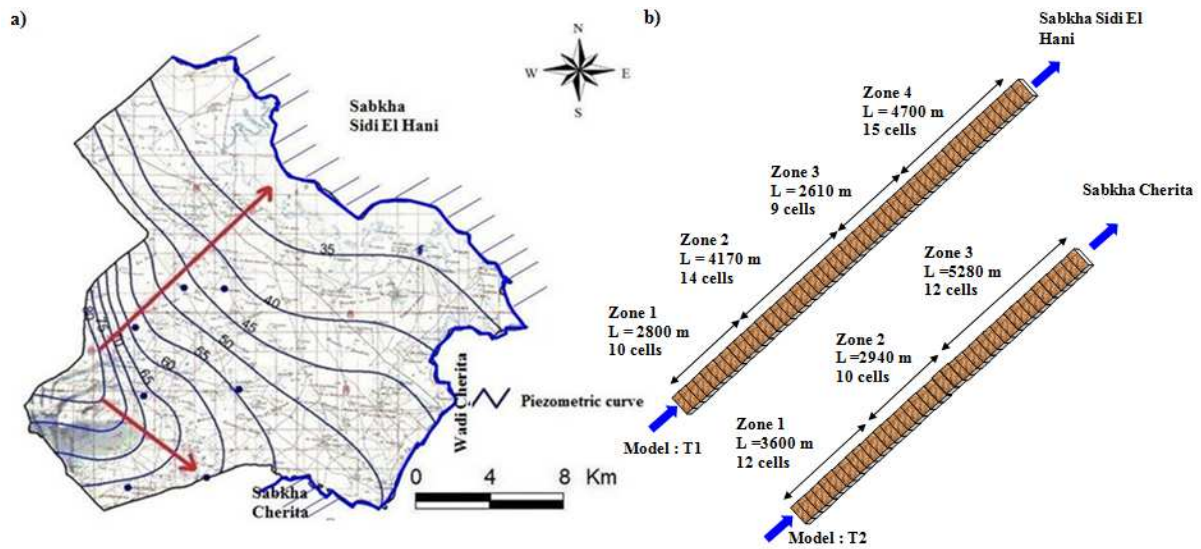


15
 16 **Figure 2:** Geological map and cross-section of the study area.

17 The depth of the water table in this shallow aquifer ranges from 3 m at the eastern part of the
 18 basin up to 26 m in the centre. The groundwater flow direction is oriented from the west to
 19 the Sabka Sidi El Hani in the north-east and to the Sabkha Cherita in the south (Fig. 3). The
 20 hydraulic heads vary between 80 and 35 m above sea level. Irregularities in the water table
 21 contours indicate high variability in the hydraulic conductivity of the alluvial aquifer from the
 22 west to the south and from the west to the east due to the heterogeneity of the sediments. In
 23 addition, the transmissivity varies between $2 \cdot 10^{-4}$ and $5 \cdot 10^{-3} \text{ m}^2 \cdot \text{s}^{-1}$, and the porosity varies
 24 between 3.5 and 4% (Dridi et al., 2013).

1

2



3

4 **Figure 3:** Hydrochemical conceptual model: a) contour map of hydraulic heads of the Sidi El
 5 Hani aquifer with flow directions illustrated by red arrows (from Dridi et al., 2013) and b)
 6 spatial discretization of the T1 and T2 transects.

7

8 2.2. Numerical reactive transport model

9 2.2.1. Governing equations of reactive mass transport

10 Most coupled reactive transport models rely on the resolution, simultaneous or not, of the
 11 partial differential equation in a saturated porous medium and the equation resulting from
 12 geochemical phenomena, which is added to the transport equation as a sink / source term.

13 The classical hypotheses of instantaneous homogeneous reactions with equal diffusion
 14 coefficients of all present aqueous species that only consider the kinetics of heterogeneous
 15 reactions make it possible to express the mass balance equation in terms of generalized (or
 16 total) concentrations Ψ_j (in mole per water mass or volume) of primary species. Under these
 17 conditions, the mass balance equation of reactive transport in a one-dimensional porous
 18 medium is written as (Lichtner, 1988; Gérard et al., 1998):

$$19 \quad \frac{\partial}{\partial t}(\phi \Psi_j) = \phi D \left(\frac{\partial^2 \Psi_j}{\partial x^2} \right) - U \frac{\partial \Psi_j}{\partial x} - \sum_{r=1}^M \alpha_{jr} \frac{\partial}{\partial t}(\phi_r \widetilde{V}_r^{-1}) \quad (j = 1, \dots, N) \quad (1)$$

20 and

$$21 \quad \frac{\partial}{\partial t}(\phi_r \widetilde{V}_r^{-1}) = v_r \quad (r = 1, \dots, M), \quad (2)$$

1 where Equation (1) refers to N aqueous primary species and Equation (2) refers to M primary
 2 species of reacting minerals. In these equations, ϕ denotes the porosity of the porous
 3 medium, ϕ_r and α_{jr} denote the volume fraction and the stoichiometric reaction coefficients,
 4 respectively, of the r^{th} mineral with molar volume \widetilde{V}_r , v_r represents the reaction rates of the
 5 irreversible reaction of minerals and fluids equivalent to the rate of precipitation or
 6 dissolution of reacting minerals r per unit of the rock and fluid system (by convention, v_r is
 7 positive for precipitation and negative for dissolution reactions), D denotes the hydrodynamic
 8 dispersion coefficient, and U denotes the Darcy velocity. The generalized concentration Ψ_j is
 9 defined according to the expression:

$$10 \quad \Psi_j = C_j + \sum_i \alpha_{ji} C_i \quad , \quad \text{with } C_i = K_i \gamma_i^{-1} \prod_{j=1}^N (\gamma_j C_j)^{\alpha_{ji}} \quad , \quad (3)$$

11 where C_j refers to the concentration of the j^{th} primary species, and the sum runs over all
 12 aqueous secondary species with concentration C_i related to the concentrations of the primary
 13 species through the mass action equation. The quantity α_{ji} denotes the molar stoichiometric
 14 coefficient of species j in secondary species i , γ is the activity coefficient of the aqueous
 15 species, and K_i denotes the equilibrium constant. Using (1) and (2), one obtains a system of
 16 (N +M) coupled nonlinear partial differential equations.

17 2.2.2. Description of the numerical model KIRMAT

18 The hydrochemical model developed in this study is based on the numerical code KIRMAT
 19 (KInetic Reaction and Mass Transport) (Gerard, 1996), which combines geochemical
 20 reactions and 1D mass transport equations. KIRMAT was developed from the thermokinetic
 21 section of the geochemical code KINDIS by integration of the reaction terms in an advective-
 22 dispersive scheme of mass transport in a saturated porous medium (Madé, 1994). The
 23 purpose of KIRMAT is to contribute to the understanding of groundwater salinization (Lucas
 24 et al., 2010), weathering processes (Lucas et al, 2017; Ackerer et al., 2018) and hydrothermal
 25 alteration (Ngo et al., 2016). It can also be used to simulate the fate of clay minerals under
 26 specific environmental conditions, such as the storage of nuclear waste (Montes et al., 2005a;
 27 2005b; Marty et al., 2009, 2010; 2006; Ngo et al., 2014).

28 The geochemical modelling of the rock-water interaction via KIRMAT requires a thorough
 29 knowledge of input parameters, such as the groundwater chemical composition, the
 30 mineralogical properties of the aquifer, and the thermodynamic and kinetic data of the

1 reaction involved. The workflow in KIRMAT is organized in three steps. In the first step, the
 2 ionic speciation (initial equilibrium) and the saturation index are calculated. During the
 3 second step, there is a perturbation of this initial partial equilibrium state by irreversible
 4 water-rock interaction due to dissolution or precipitation of minerals (reaction term v_r , see
 5 Eq. 2), which results in either supplying or removing elements from the aqueous solution.
 6 Finally, the (N+M) partial differential equations (1) and (2) are solved simultaneously with a
 7 one-step algorithm. The mass transport equations are solved using a finite difference
 8 approximation in an explicit scheme.

9 *Saturation index and ionic speciation*

10 The saturation index (SI) of the reactions occurring between the aqueous species and
 11 minerals is defined by Equation 4:

$$12 \quad SI_i = \log \frac{Q_i}{K_i}, \quad (4)$$

13 where Q_i denotes the ion activity product and K_i denotes the thermodynamic equilibrium
 14 constant. If the water sample is completely saturated with the dissolved mineral, SI equals
 15 zero. Positive values of SI indicate super-saturation under which the mineral would tend to
 16 precipitate; negative values indicate under-saturation and mineral dissolution.

17 For each species and mineral in the studied system, the ion activity products are obtained by
 18 applying the corresponding activity coefficients:

$$19 \quad Q_i = \prod_{i \in E} [a_i]^{\alpha_{ij}} = \prod_{i \in E} [m_i \gamma_i]^{\alpha_{ij}}, \quad (5)$$

20 where a_i denotes the activity of species i , m_i denotes the molality, γ_i denotes the activity
 21 coefficient, E represents the basic species assemblage of the study system and α_{ij} is the
 22 stoichiometric coefficient of the specie i in the complex j . In our current study, the activity
 23 coefficient γ_i has been fitted with the Debye-Hückel model (6), which is largely used in
 24 geochemical models (Debye-Hückel, 1923):

$$25 \quad \log \gamma_i = \frac{A Z_i^2 \sqrt{I}}{1 + s_i B \sqrt{I}} + CI, \quad (6)$$

26 where A , B and C denote the Debye-Hückel constants, s_i , I and Z_i denote the size, the ionic
 27 strength of the solution and the electric charge, respectively, of the specie i .

1 **Water-rock interaction**

2 In KIRMAT, the interaction between water and rock (see Eq. 2) involves dissolution and
3 precipitation, which are controlled by many factors, including the mineral surface, the
4 solution composition, the temperature and the degree of saturation of the aqueous solution
5 with respect to the studied mineral. In our study, only the dissolution of minerals was
6 modelled by irreversible kinetics. The kinetic of rock dissolution r_d (in mole per water mass)
7 is quantified by (G erard, 1996):

$$8 \quad r_d \stackrel{\text{def}}{=} v_r = k_{d,r} S_r^{\text{eff}} \alpha_H^n \left(1 - \frac{Q_r}{K_r}\right), \quad (7)$$

9 where $k_{d,r}$ denotes the dissolution rate constant ($\text{mole m}^{-2} \text{ year}^{-1}$) of the reactive mineral r , S_r^{eff}
10 stands for the reactive surface area of mineral r ($\text{m}^2 \cdot \text{kg}_{\text{H}_2\text{O}}^{-1}$), α_H^n denotes the proton activity
11 where n depends on the pH of the solution, Q_r is the ion activity product of reactive mineral r
12 and K_r denotes the thermodynamic equilibrium constant of the hydrolysis reaction of mineral
13 r at a given temperature and pressure.

14 Finally, the dynamic system is discretized over a time step Δt until the time $t + \Delta t$, which is
15 equal to the simulation time requested by the user. A self-adjusting numerical time step was
16 used during the simulations. Furthermore, the KIRMAT code can also describe the feedback
17 effect of the chemical and mineralogical evolution of the permeability at any node of the
18 mesh due to the dissolution and precipitation reaction, which can modify the pore geometry
19 (Laabidi and Bouhlila, 2015). The intrinsic permeability k (m^2) is updated after each time
20 step as follows (Gerard, 1996):

$$21 \quad k = C_0 \left[\phi^{c-1} \left(\frac{\phi^3}{(1-\phi)^2 S^2} \right) \right]^2, \quad (8)$$

22 where C_0 , c , ϕ and S denote the cementing factor, an experimental constant, and the porosity
23 of the porous medium and the grid cell surface in contact with the adjacent cell (m^2),
24 respectively.

25 **2.2.3. Model domain**

26 According to the flow direction of the groundwater, two transects T1 and T2 are chosen to
27 model the behaviour of the aquifer. The first transect is located from the lower (inlet)
28 boundary near El Gussat Mountain to the Sabkha Sidi El Hani. The second transect is
29 oriented to the Sabkha Cherita (Fig. 3).

1 The lengths of transect T1 and T2 are 16 km and 14 km, respectively. The two transects are
2 discretized with a horizontal spacing of 300 m-long meshes. Based on the area and the
3 geological characteristics (see Fig. 2), T1 contains four zones, whereas T2 is composed of
4 three zones. The mineralogical compositions involved in the modelled transects are halite,
5 calcite, gypsum, anhydrite, dolomite, illite and quartz. All of the zones of each transect are
6 assumed to have the same mineralogy. The only exceptions are the first and second zones of
7 T1 and T2, where halite is not present because the ion ratios of Na^+ to Cl^- of the groundwater
8 samples are lower than 1. This relationship suggests that the concentrations of both ions are
9 not due to halite dissolution.

10 The simulation covered 50 and 100 year periods. These periods were chosen to explain the
11 chemical composition of groundwater in 2015, which was used as the initial state. The two
12 modelled transects are presented in Figure 3. In our study, the mineralogical compositions are
13 considered homogenous in each transect zone due to the non-availability of the data. In
14 addition, the geologic map showed significant lithological variation. All numerical
15 simulations are performed at a constant temperature of 25°C because the average of the
16 temperature measured in the different samples of groundwater is of the order of 25°C .

17

18 *2.2.4. Initial and boundary conditions of the model*

19 The initial conditions (IC) of our model are based on the average of the chemical composition
20 of all observation wells located along each streamline. Concentrations of the upstream
21 boundary (UB) were applied as fixed-concentrations corresponding to a 1st order type, or
22 Dirichlet boundary. The measured concentrations of the first observation well located at the
23 upstream of the modelled section were used as the prescribed concentrations. The
24 downstream boundary (DB) was set as a free flux boundary.

25 The physical and chemical characteristics of the injected fluid in T1 and T2 are reported in
26 Table 1. The measurement of physical parameters such as pH and temperature (T) were
27 performed in the field, whereas the analyses of chemical compositions of the injection fluid
28 in both T1 and T2 were performed in the laboratory in accordance with the standard methods
29 of the American Association of Public Health (APHA, 1995). Calcium (Ca^{2+}) and magnesium
30 (Mg^{2+}) concentrations were determined by the complexometric method. Sodium (Na^+) and
31 potassium (K^+) concentrations were measured by atomic absorption spectrometry. Sulphate
32 (SO_4^{2-}) concentrations were determined by the gravimetric method, and chloride (Cl^-) and

1 bicarbonate (HCO_3^-) concentrations were quantified by titration. Validation of the chemical
 2 analysis results was performed by verification of the error percentage, which was judged
 3 acceptable if the value is less or equal 5% (Appelo and Postma, 2005).

4 **Table 1:** Physical and chemical compositions of water chosen at the upstream boundary (UB)
 5 and downstream boundary (DB) of T1 and T2, compared to the initial conditions (IC) in
 6 2015.

Parameter	T1			T2		
	UB	IC	DB	UB	IC	DB
pH	7.0	8.4		7.0	8.0	
T(°C)	25.0	25.0		25.0	25.0	
Element	Concentration (mmol/kg _{H2O})					
	Free flux			Free flux		
Ca	7	16		7	15	
Mg	15	12		15	13	
Na	40	59		40	39	
K	1	1		1	1	
Cl	30	46		30	31	
S	30	30		30	24	
C	3	3		3	5	

7

8 *2.2.5. Model parameters*

9 *Mineralogical composition and reactive surface*

10 To study the geochemical processes between the rock and groundwater in the Sidi El Hani
 11 aquifer, it is crucial to define the mineralogical composition of the aquifer. Hence, a borehole
 12 profile was performed in the study area with a depth of 30 m. There were 27 core samples
 13 collected along the profile. Rock samples were dried before undergoing mineralogical
 14 analysis. X-ray diffraction analysis of the cuttings highlights that the Sidi El Hani reservoir is
 15 heterogeneous. The reservoir contains quartz, gypsum, halite, anhydrite, dolomite, and calcite
 16 with 56%, 10%, 4%, 3%, 3% and 14% volume fractions, respectively (Table 2). In addition,
 17 the X-ray diffraction analysis underlined that the reservoir contains illite in a volume fraction
 18 of approximately 10%. Because illite has a low cation exchange capacity compared to the
 19 other clay minerals (Sparks, 2003), sorption effects are neglected in our study. Heterogeneous

1 reactions modelled with KIRMAT thus only include dissolution and precipitation processes
 2 between rock and water.

3 **Table 2:** Mineralogical composition and corresponding volume fraction of the Sidi El Hani
 4 reservoir.

Mineral	Structural formula	Volume fraction (%)
Quartz	SiO ₂	56
Gypsum	Ca SO ₄ .2H ₂ O	10
Halite	NaCl	4
Anhydrite	CaSO ₄	3
Dolomite	Ca Mg (HCO ₃) ₂	3
Calcite	CaCO ₃	14
Illite	Si _{3.5} Al _{2.3} Mg _{0.25} O ₁₀ (OH) ₂ K _{0.6}	10

5 The reactive surface of the minerals that is involved in both dissolution and precipitation
 6 reactions is often difficult to estimate because of insufficient knowledge of some natural
 7 factors. Note that this is one of the most sensitive parameters of the modelling of geochemical
 8 systems (Wilson et al., 2015). Its estimation is often questionable due to certain ambiguities,
 9 such as the roughness of the surface and the changing of the surface area throughout the
 10 reaction progress (Savage et al., 2002; Molins et al., 2012). Methods for measuring reactive
 11 surfaces have been discussed in numerous studies (Gérard, 1996; Kieffer et al.; 1999; Marty,
 12 2006; Ngo et al., 2014). In our study, we assume that the reactive surface area of the involved
 13 minerals remains constant during the numerical simulation. The reactive surface S_r^{eff} (m² kg⁻¹
 14 H₂O) was calculated as follows:

$$15 \quad S_r^{\text{eff}} = V_r \frac{S_{\text{cube}}}{V_{\text{cube}}}, \quad (9)$$

16 where V_r (m³.kg⁻¹) denotes the volume of the reactive mineral per kilogram of water, and
 17 S_{cube} (m²) and V_{cube} (m³) stand for the surface and the volume of the cube, respectively. V_r
 18 was calculated by

$$19 \quad V_r = F_r \frac{(1-\phi)*1000/\rho}{\phi}, \quad (10)$$

20 where F_r and ρ represent the volume fraction and the volumetric mass (kg.m⁻³) of the mineral,
 21 respectively.

1 It is assumed that all minerals have a cubic shape. Therefore, the long sides should be 10^{-3} m.
 2 However, long sides of clay minerals are assumed to be $1 \mu\text{m}$ because they are formed with a
 3 smaller size than the other minerals (Meunier, 2006). The porosity of the aquifer was
 4 estimated to be 0.04. The calculated reactive surfaces of the minerals are shown in Table 3.

5 **Table 3:** Length and area of reactive surfaces of the minerals.

Mineral	Long sides of the mineral (m)	Reactive surface area ($\text{m}^2 \cdot \text{kg H}_2\text{O}^{-1}$)
Quartz	10^{-3}	8.566
Gypsum	10^{-3}	1.000
Halite	10^{-3}	0.856
Anhydrite	10^{-3}	0.428
Dolomite	10^{-3}	0.571
Calcite	10^{-3}	0.713
Illite	10^{-6}	0.576

6 ***Thermodynamic and kinetic parameters***

7 The thermodynamic parameters of the minerals used in our numerical studies, at a
 8 temperature of 25°C , are summarized in Table 4 for six primary minerals and one secondary
 9 mineral.

10 **Table 4:** Parameters of the modelled primary and secondary minerals.

Mineral	Structural formula	Log K (25°C)
Illite	$\text{Si}_{3.5}\text{Al}_{2.3}\text{Mg}_{0.25}\text{O}_{10}(\text{OH})_2\text{K}_{0.6}$	-43.192
Gypsum	$\text{CaSO}_4 \cdot 2\text{H}_2\text{O}$	-4.630
Anhydrite	CaSO_4	-4.390
Halite	NaCl	1.570
Dolomite	$\text{CaMg}(\text{CO}_3)_2$	-18.28
Calcite	CaCO_3	-8.370
Quartz	SiO_2	-3.999

11 (Gérard et al., 1998)

12 Note that kinetic data are less available in the literature than thermodynamic data, mainly for
 13 the precipitation of reactive minerals. Considering Equation 7, the dissolution rates of
 14 primary or secondary minerals were determined from data sets proposed by Palandari and

1 Kharaka (2004), which are based on kinetic values at 25°C and an activation energy term
 2 (Table 5).

3 **Table 5:** Kinetic constants of dissolution reactions of primary and secondary minerals at
 4 25°C.

Mineral	Acidic conditions			Neutral conditions			Basic conditions		
	^a log k	^b E	^c n	^a log k	^b E	n	^a log k	^b E	^c n
Illite	-11,31	65,4	0,77	-13,18	22,20	-	-17,05	17,90	-0,47
Gypsum	-	-	-	-3,19	14,30	-	-	-	-
Anhydrite	-	-	-	-6,50	31,30	-	-	-	-
Halite	-	-	-	-0,21	7,40	-	-	-	-
Dolomite	-3,19	36,1	0,50	-7,53	52,20	-	-5,11	34,80	0,50
Calcite	-0,30	14,40	1,00	-5,81	23,50	-	-3,48	35,40	1,00

5 a: rate constant k computed at 25°C; b: Arrhenius activation energy E (kJ mole⁻¹); c: reaction order n with
 6 respect to H⁺.

7 To model dissolution kinetics at any temperature, KIRMAT code uses the following
 8 expression for mineral dissolution controlled by surface reactions (Madé et al., 1994):

$$9 \quad r_{d,i} = S_{eff}^m \left(1 - \frac{Q_i}{K_i}\right) \left[\begin{array}{l} k_{25}^{Acid} \exp \left[\frac{-E_a^{Acid}}{R} \left(\frac{1}{T} - \frac{1}{298.15} \right) \right] \alpha_{Acid}^{n_{Acid}} \\ + k_{25}^{Neutral} \exp \left[\frac{-E_a^{Neutral}}{R} \left(\frac{1}{T} - \frac{1}{288.15} \right) \right] \\ + k_{25}^{Base} \exp \left[\frac{-E_a^{Base}}{R} \left(\frac{1}{T} - \frac{1}{298.15} \right) \right] \alpha_{Base}^{n_{Base}} \end{array} \right], \quad (11)$$

10 where $r_{d,i}$ represents the dissolution rate controlled by the surface reaction (mol year⁻¹ kg⁻¹
 11 ^lH₂O), and S_{eff} is the reactive surface area for a given mineral i. Q_i and K_i denote the activity
 12 product and the thermodynamic equilibrium constant at the given temperature, respectively.
 13 k_{25}^{Acid} , $k_{25}^{Neutral}$ and k_{25}^{Base} represent the dissolution rate constant at 25°C and pH=0, for
 14 acidic, neutral and basic conditions, respectively. n_{Acid} and n_{Base} are the reactions order with
 15 respect to the pH of the solution, R the gas constant (J.K⁻¹ mol⁻¹) and T the temperature (K).

16 *Hydrodynamic parameters*

17 The hydrodynamic parameters of the Sidi El Hani aquifer were derived from the
 18 hydrogeological model created by Dridi et al. (2013) using Visual Modflow. A Darcy
 19 velocity of approximately 91 and 152 m.year⁻¹ for T1 and T2, respectively, were chosen
 20 according to hydraulic conductivity and hydraulic gradient measurements obtained from the

1 contour map of hydraulic heads of the Sidi El Hani aquifer. In addition, the numerical value
 2 of the porosity for both transects (T1 and T2) was estimated to be 4% (Dridi et al., 2013).
 3 However, the estimated values of hydraulic conductivity were approximately 30×10^{-5} and
 4 $9 \times 10^{-5} \text{ m s}^{-1}$ for T1 and T2, respectively.

5 2.2.6. Model calibration and sensitivity study

6 The calibration of the model was carried out by minimizing the differences between observed
 7 and simulated groundwater concentrations. The comparison was made with concentration
 8 data measured in March and April 2015 in numerous observation wells located along both
 9 transects. Using the reactive surface areas given in Table 3 and the initial dissolution rate
 10 constants (Table 5), the preliminary simulation led to an overestimation or underestimation of
 11 the chemical element concentrations. Hence, it was decided to adjust the dissolution rates of
 12 minerals, which are often different than those estimated by many authors (Kim, 2002; White
 13 and Brantely, 2003; Maher et al., 2006). In the case of carbonates, we used the dissolution
 14 rate constants for basic conditions. The adjusted dissolution rates obtained for gypsum,
 15 anhydrite, calcite, dolomite and halite are shown in Table 6. They are in the range proposed
 16 by Palandari and Kharaka (2004).

17 **Table 6:** Initial and adjusted reactive dissolution rates.

Mineral	Dissolution rate Log k (mol years⁻¹ kgH₂O⁻¹)	Adjusted dissolution rate Log k (mol years⁻¹ kgH₂O⁻¹)
Gypsum	-2.79	-1.92
Anhydrite	-3.19	-1.30
Halite	-0.21	-1.69
Calcite	-3.00	-1.92
Dolomite	-3.11	-3.15

18 To obtain a good match between the computed and observed chemical composition, a large
 19 number of trial-and-error runs were performed. The response of the model was evaluated by
 20 the root-mean-square-error (RMSE) between computed and observed concentrations of each
 21 monitoring point (Eq. 12):

$$22 \text{ RMSE} = \sqrt{\frac{1}{n} \sum (O_i - C_i)^2}, \quad (12)$$

1 where n denotes for the number of observations, and O_i and C_i are the measured and
2 calculated groundwater concentrations of species i ($\text{mol kg}_{\text{H}_2\text{O}}^{-1}$).

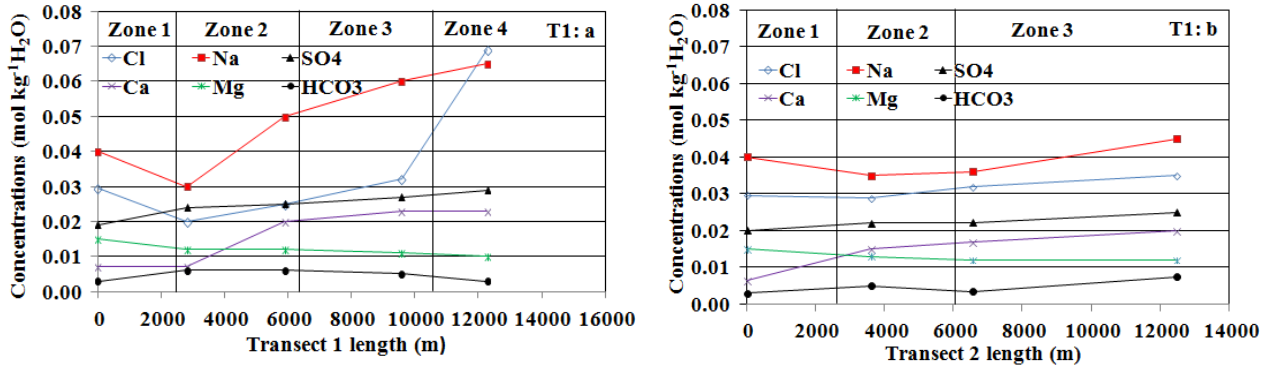
3 Sensitivity analysis was performed individually to identify the model input parameters that
4 may have an influence on the reactive mass transport in the aquifer. This allows us to
5 understand and interpret the numerical results of the hydrochemical model. The sensitivity
6 study was conducted for three specific cases: i) variation of the volume fraction of halite ; ii)
7 variation of the chemical composition of incoming water and (iii) variation of the Darcy
8 velocity.

9 **3. Results and discussion**

10 *3.1. Observed concentrations of major elements*

11 The spatial variation of dissolved species measured in the groundwater samples along the two
12 transects T1 and T2 is shown in Figure 4. The concentration of the major elements are Cl
13 ($0.02\text{-}0.07 \text{ mol.mol.kg}_{\text{H}_2\text{O}}^{-1}$), Na ($0.03\text{-}0.07 \text{ mol.kg}_{\text{H}_2\text{O}}^{-1}$), SO_4 ($0.019\text{-}0.020 \text{ mol.kg}_{\text{H}_2\text{O}}^{-1}$),
14 Ca ($0.007\text{-}0.023 \text{ mol.kg}_{\text{H}_2\text{O}}^{-1}$), Mg ($0.010\text{-}0.015 \text{ mol mol.kg}_{\text{H}_2\text{O}}^{-1}$), HCO_3 (0.003-
15 $0.006 \text{ mol.kg}_{\text{H}_2\text{O}}^{-1}$), and K ($0.001 \text{ mol mol.kg}_{\text{H}_2\text{O}}^{-1}$) with the ionic sequence $\text{Na}>\text{Ca}>\text{Mg}>\text{K}$
16 and $\text{Cl}>\text{SO}_4>\text{HCO}_3$. All of the water samples show a large deficit of HCO_3 and K. However,
17 a great excess of Cl and Na has been shown in zones 3 and 4 of T1 and in zone 3 of T2
18 compared to the first and second zones. In these areas groundwater is characterized by a high
19 salinity with a concentration of total dissolved solids (TDS) above 6 g L^{-1} . In fact, the history
20 of the salinity of the given aquifer system stems from the geomorphology of the area during
21 the Quaternary. Essefi et al. (2013) showed that the Sidi El Hani-Cherita system had a salty
22 heritage in the Tunisian Sahel area. Furthermore, they suggested two hypotheses for the
23 origin of the salt. The first is linked to the halokinesis activities of the Triassic evaporitic
24 sedimentation in the subsurface. The second states that the Messinian salinity crisis has left
25 huge quantities of salt and salt water in the Sidi El Hani aquifer. This saline subsurface is
26 until now influencing the behaviour of the area as a whole. Through groundwater
27 convergence, the salts are accumulated within depression zones. Recently, M'nassri et al.
28 (2016 and 2018) investigated the salinization problem of the unconfined aquifer of Sidi El
29 Hani. Their studies showed that the high groundwater salinization is principally due to the
30 rock-water interaction, including chemical and physical reactions, such as dissolution and
31 precipitation. These reactions probably altered not only the chemical compositions of the
32 rocks and the quality of the groundwater, but they also contributed to the formation of new
33 minerals along the flow pathway (Edmunds et al., 2002; Rajmohan and Elango, 2004;

1 Meredith et al., 2012; Pacheco and Van der Weijden, 2014). Additionally, measured SO₄ and
 2 Ca concentrations are increased, except in the water samples of zone 1. These two ions
 3 appear to be inherited from the same rock. The variation of the chemical elements in the
 4 different zones seems to be determined by the nature of the geology.

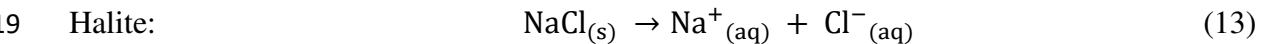


5 **Figure 4:** Distribution of Cl, Na, SO₄, Ca, Mg and HCO₃ ions measured in the groundwater
 6 along (a) transect 1 (T1) and (b) transect 2 (T2).

7 3.2. Simulated concentrations of dissolved species along the transects at different times

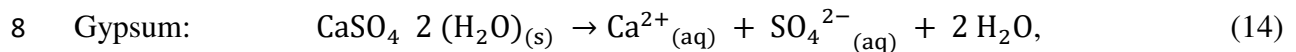
8 The calculated dominant aqueous compositions, including sodium, calcium, magnesium,
 9 sulphate and chloride ions, are presented along the two transects in Figure 5 and are
 10 compared to the measured concentrations. There is globally a good agreement between
 11 calculated and measured concentrations after 100 years.

12 It is found that the concentrations of Cl and Na increase progressively with travel distance.
 13 They reach values of 0.08 mol kg⁻¹ H₂O and 0.09 mol kg⁻¹ H₂O in T1 and value of 0.055 mol
 14 kg⁻¹ H₂O and 0.062 mol kg⁻¹ H₂O in T2, respectively. The increased concentrations are
 15 observed in cells containing the mineral halite. Therefore, the interaction between halite and
 16 groundwater has a strong influence on the spatiotemporal evolution of dissolved sodium
 17 chloride. Assuming the dissolution of halite, the geochemical process can be expressed by
 18 halite (Eq. 13), gypsum (Eq. 14) and anhydrite (Eq. 15).

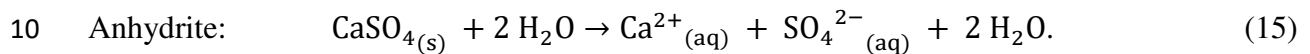


20 The dissolved concentrations calculated in T1 and T2 after 30, 50 and 100 years show a slight
 21 decrease over time. This can be explained by a decrease in mineral mass relative to its
 22 reactive surface (Kieffer et al., 1999; Colon et al., 2004; Prikryl et al., 2017) during the
 23 dissolution process of halite. In addition, in comparing the two transects, the Cl and Na
 24 concentrations observed in T2 are lower, due to the presence of halite only in the third zone,
 25 which is very short compared to the overall length of zones 2, 3 and 4 in transect T1.

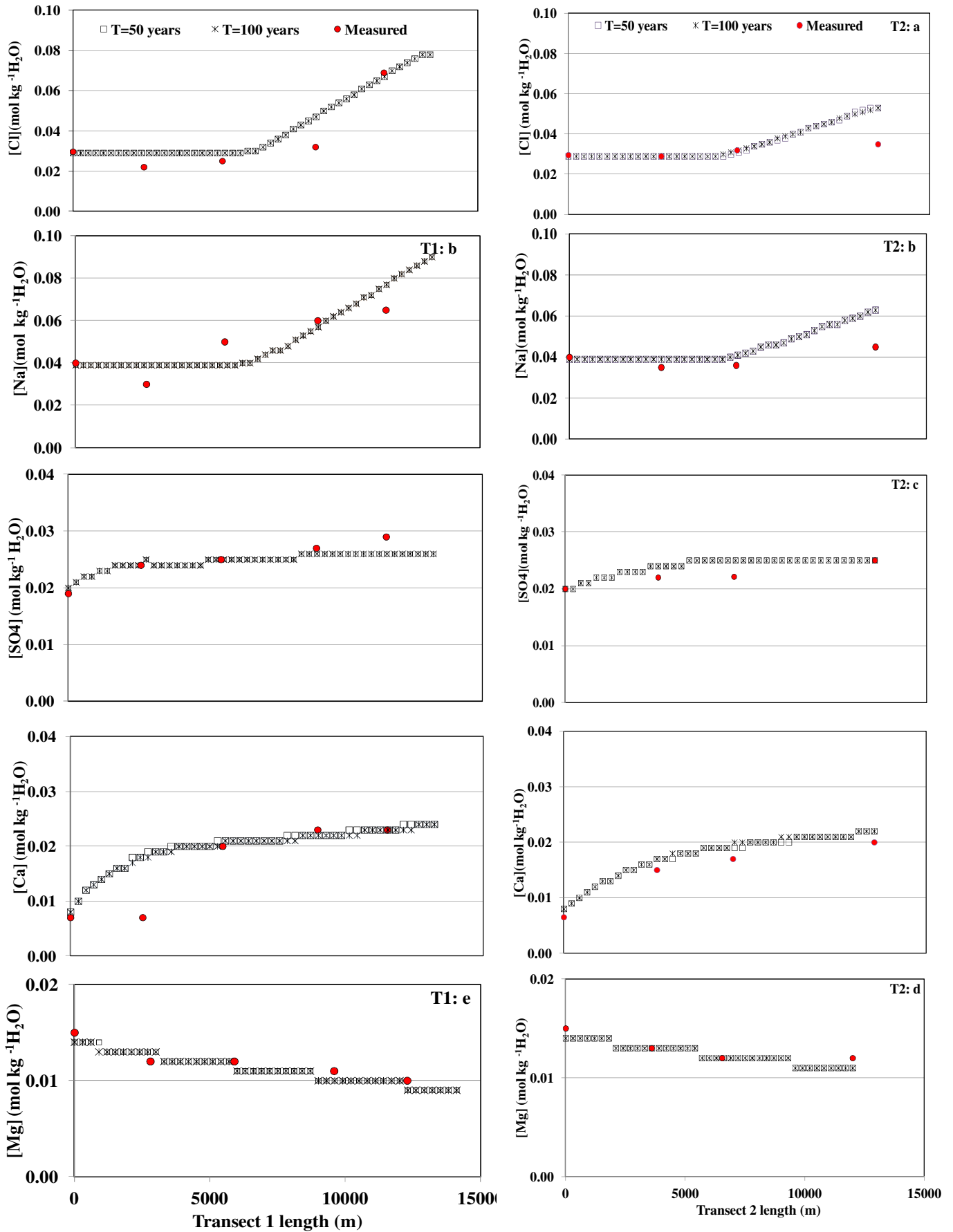
1 However, the calculated SO₄ and Ca concentrations generally increase with travel distance
2 (Fig. 5). The most logical source of these ions is the dissolution of gypsum and anhydrite
3 according to equations (14) and (15) (Jones et al., 1999; Wu et al., 2009). The gypsum and
4 anhydrite minerals both release one mole of SO₄ and one mole of Ca. However, their
5 temporal evolution is different. The SO₄ and Ca concentrations calculated at T1 and T2 do
6 not vary between 50 and 100 years. The Ca release is very likely due to the precipitation of
7 calcite and/or dolomite:



9



11 Furthermore, the spatial distribution of the calculated Mg concentration can be characterized
12 as follows: a decrease in concentration from the first zone to the fourth zone of T1, while the
13 concentrations are more or less the same along transect T2. The decrease in concentrations as
14 a function of travel distance is likely due to the precipitation of dolomite, which can occur
15 along the flow path of T1.



1 **Figure 5:** Spatiotemporal evolution of selected dissolved species along transects T1 and T2:
 2 (a) chlorides, (b) sodium, (c) sulphates, (d) calcium, and (e) magnesium.

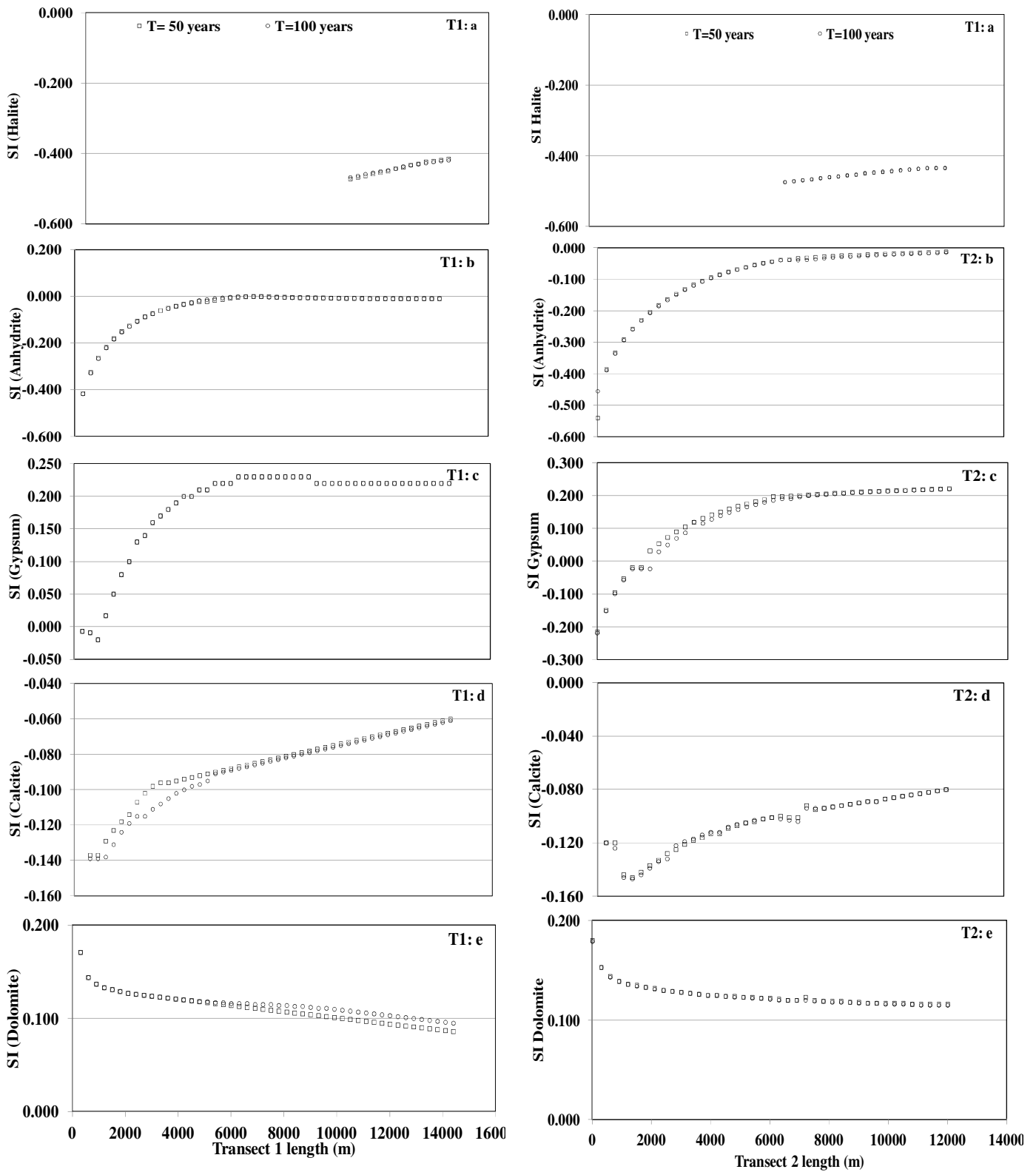
1 *3.3 Numerical modelling of the saturation indexes*

2 The dissolution and precipitation of carbonate minerals and evaporites are determined by the
3 saturation level of the water solution. The results of the simulation of these processes are
4 shown in Figure 6. Dissolution of halite, anhydrite, gypsum and calcite minerals is very high
5 in the first zones of each transect.

6 The computed saturation index (SI) of halite is lower than zero everywhere, which shows that
7 the salt rock is not saturated. However, the saturation index increases at the downstream
8 boundary because of the washing out of the dissolved quantity of halite along the flow path.
9 The SI values of anhydrite are negative or close to zero, which suggests that this mineral is in
10 equilibrium with water, especially in the downstream zones of the modelled transects.
11 However, the saturation index of gypsum increases gradually until it reaches 0.23 and 0.21 in
12 T1 and T2, respectively. The positive values indicate that a saturated state of this mineral is
13 achieved where the ions accumulate in the water solution.

14 The saturation indexes computed for calcite and dolomite are in the range of -0.14 and -0.06
15 and 0.08 and 0.20 for T1 and in the range of -0.16- and -0.08 and 0.12 and 0.2 for T2,
16 respectively. This clearly reflects the conversion from under-saturation of calcite to the over-
17 saturation of dolomite. The lixiviation of the calcite releases the moles of Ca, which are then
18 involved in the precipitation of dolomite. Calcite would thus be scarce, as water could not
19 reach the necessary saturation.

20

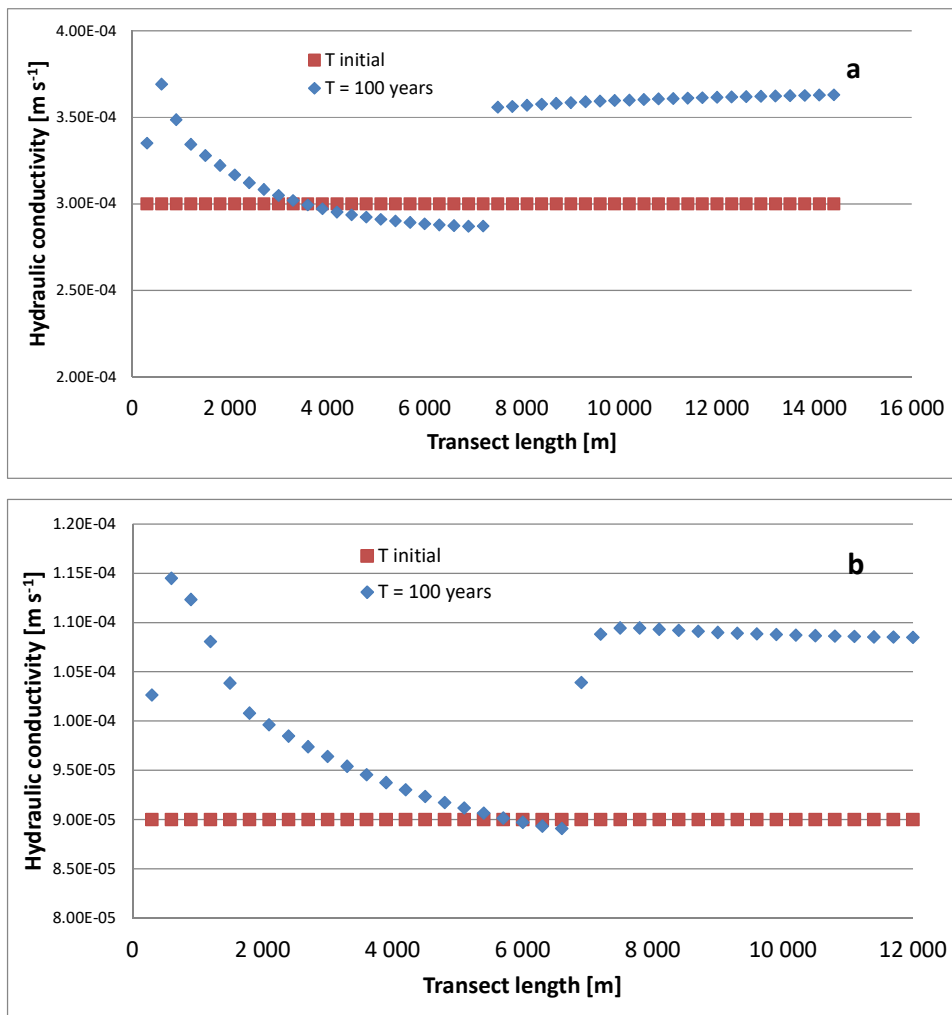


1 **Figure 6:** Numerically calculated saturation index (SI) as a function of travel distance and
 2 time for (a) halite, (b) anhydrite, (c) gypsum, (d) calcite, and (e) dolomite.

1 One may conclude that the most important reactions that can occur in the groundwater of the
 2 Sidi Hani aquifer are the dissolution of halite, anhydrite and calcite, the dissolution and
 3 precipitation of gypsum and the precipitation of dolomite. Water may instantaneously react
 4 with halite, anhydrite and gypsum and then differently increase the concentrations of Cl, Na,
 5 and SO₄ in the water, which leads to an increase in the total dissolved solids. In addition, in
 6 zones where anhydrite is present, its dissolution could provoke precipitation of gypsum.

7 *3.4. Spatiotemporal evolution of permeability*

8 The final hydraulic conductivity profile in both modelled transects T1 and T2 is shown in
 9 Figure 7. There is a change in permeability after 100 years of interaction between the water
 10 and minerals observed in the two transects. They varied between 2.9×10^{-4} and 3.7×10^{-4} m s⁻¹
 11 and between 9×10^{-5} and 11.4×10^{-5} m y⁻¹ for T1 and T2, respectively.



12 **Figure 7:** Numerically calculated hydraulic conductivity distribution in (a) transect 1 and (b)
 13 transect 2.

1 Globally, there is an increase of the hydraulic conductivity. In the first zones of each transect
2 this increase is due to the high dissolution of anhydrite and calcite minerals, then a decrease
3 occurs due to dolomite precipitation. Further, downstream of zone 2, the dissolution of halite
4 leads to an increase of hydraulic conductivity.

5 *3.5. Model calibration*

6 Different numerical runs were performed to quantify the numerical values of the reactive
7 surface and the kinetic rate of mineral dissolutions and to test their influence on the chemical
8 composition of the groundwater. The best fit of the measured chemical compositions was
9 obtained for the adjusted dissolution rates (Table 6). For the comparison, we used the
10 numerical results after 100 years. The model provides a good estimate of chemical elements
11 for the tow modelled transects T1 and T2 with a RMSE value of approximately 0.01 for all of
12 the chemical species. Note that the measured concentrations of Cl, Na, Ca, SO₄ and Mg
13 concentrations for T1 vary between 0.03 and 0.07, 0.04 and 0.07, 0.007 and 0.023, 0.019 and
14 0.029, and 0.015 and 0.011 mol kg⁻¹ H₂O, respectively.

15 For transect T2, the measured concentrations of Cl, Na, Ca, SO₄ and Mg vary between 0.03
16 and 0.04, 0.04 and 0.05, 0.007 and 0.020, 0.020 and 0.025, and 0.015 and 0.012 mol kg⁻¹
17 H₂O, respectively. The numerical results were close to the field data. The obtained correlation
18 coefficients show an acceptable correlation between measured and simulated chemical
19 concentrations for T1 and T2 (Table 7).

20 **Table 7:** Correlation coefficients.

	Transect 1	Transect 2
Cl	0.86	0.77
Na	0.70	0.77
Ca	0.64	0.99
Mg	0.81	0.83
SO ₄	0.93	0.63

21

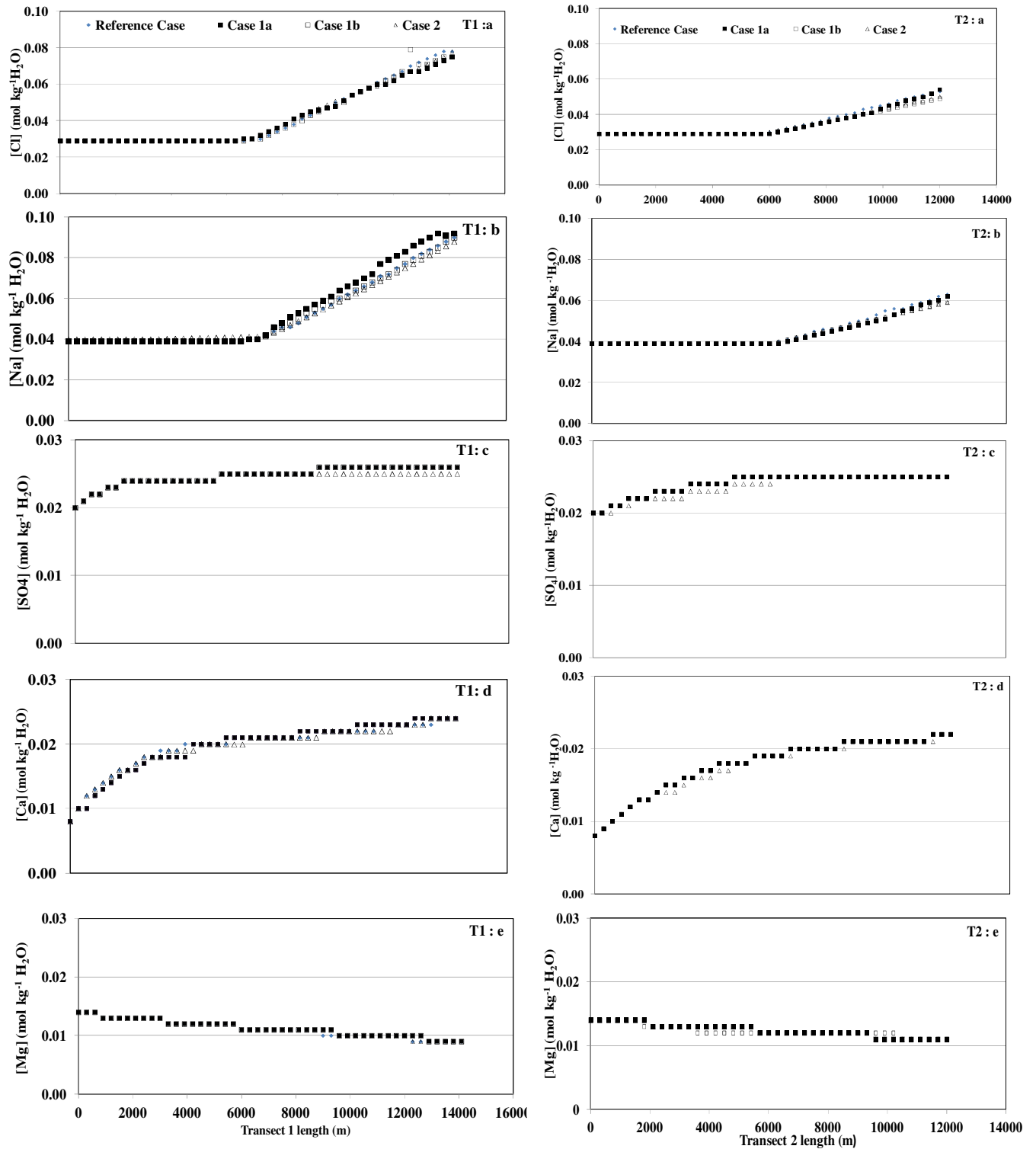
22 *3.6. Sensitivity studies*

23 Water-rock interaction is the major factor responsible for groundwater salinity. Its influence
24 was first analysed using two numerical studies that analysed (1) the variation of volume

1 fractions of minerals and (2) the chemical composition of the injected water flux. The
2 sensitivity of the simulated results of both cases was tested by varying their initial optimised
3 values and taking as reference the previous numerical results obtained at t=100 years. The
4 results of these two sensitivity studies are presented and compared to the reference results in
5 Figure 8.

6 In the first sensitivity study, we increased (case 1a) and decreased (case 1b) the volume
7 fraction of minerals up to 10%. It was shown that the dissolved ions, such as chlorides,
8 calcium, magnesium and sulphates, are not sensitive to this parameter. If sodium is a little bit
9 more sensitive, its response to the volume fraction variation remains lower than 10%. In the
10 second sensitivity case, the chemical composition of the injected water flux was replaced by
11 the chemical composition of the first observation well located upstream of each transect. Here
12 also, the calculated dissolved concentrations of major elements do not differ significantly
13 from those of the reference case and highlight the finding that the composition of the water at
14 the upstream boundary is not a sensitive model parameter.

15



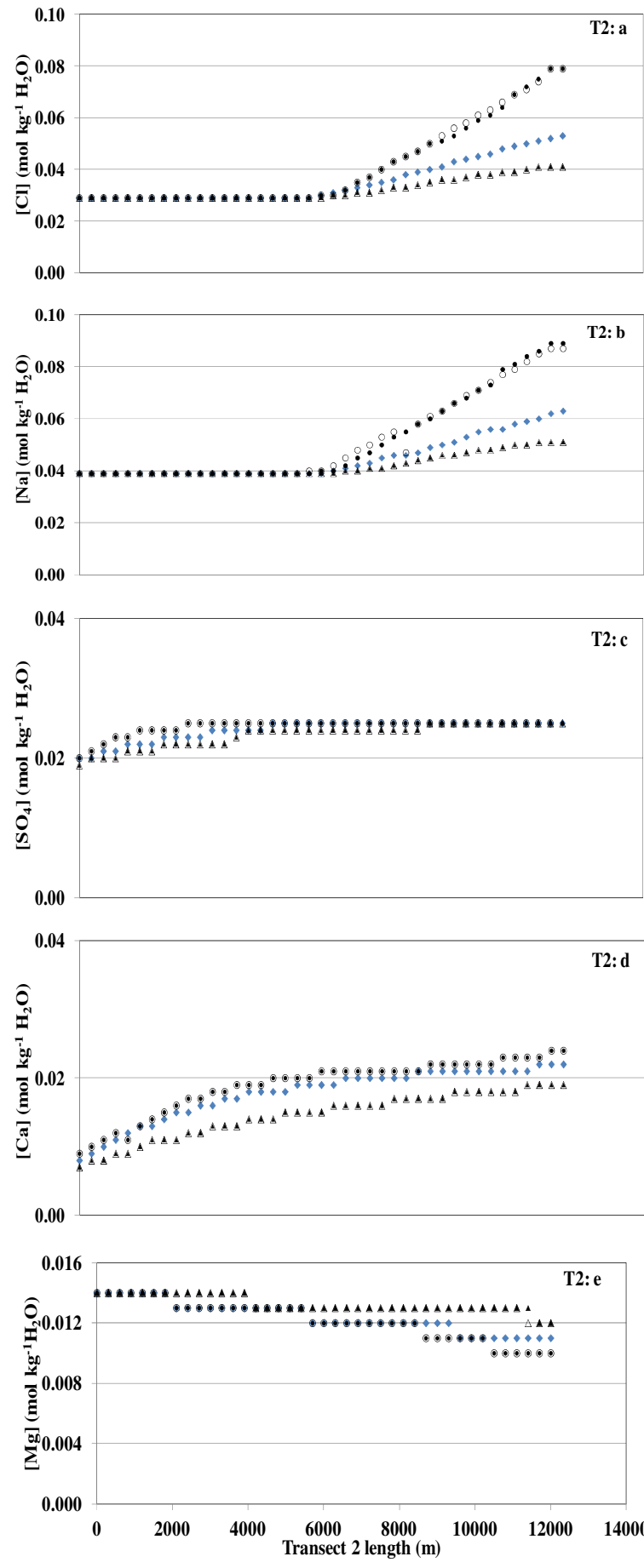
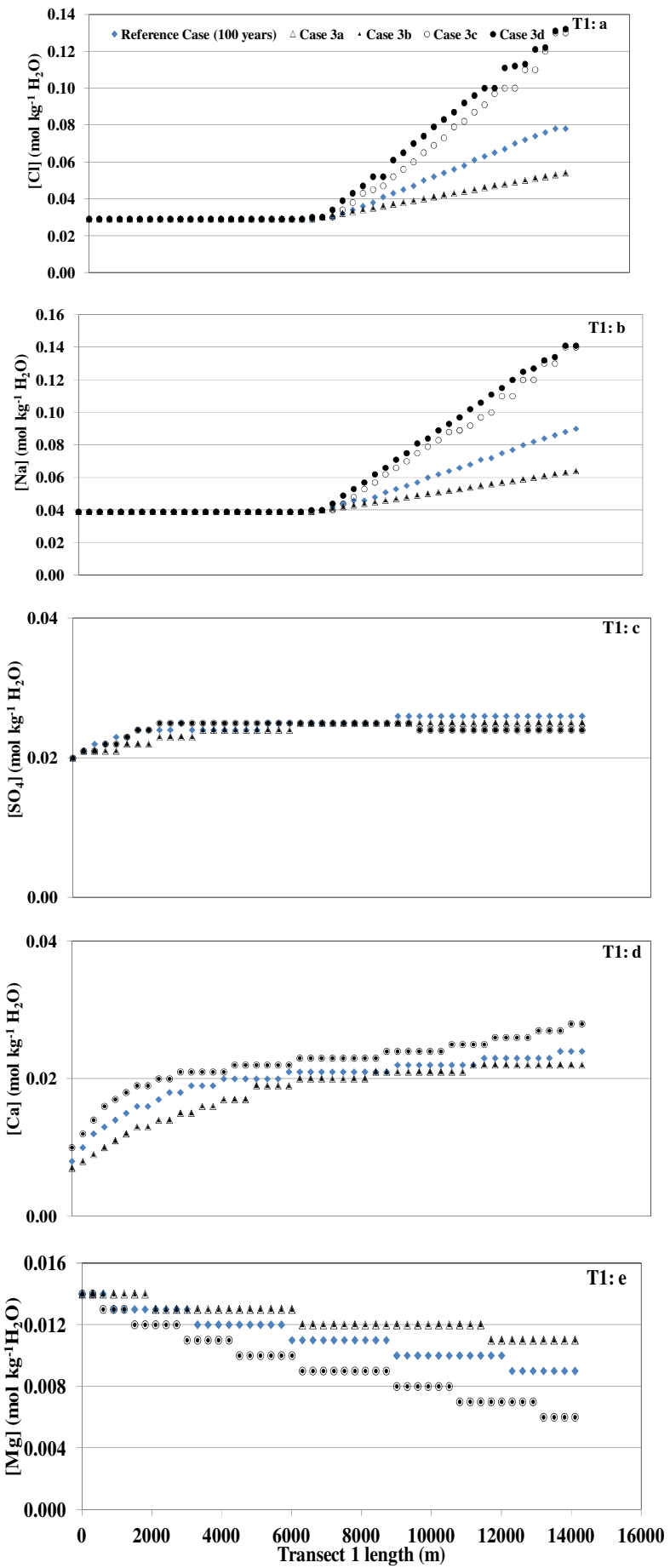
1 **Figure 8:** Sensitivity study of the influence of the volume fraction of minerals (cases 1a and
2 1b) and the chemical composition of injected water flux (case 2) on modelled dissolved major
3 elements of the ground water: (a) Cl, (b) Na, (c) SO₄, (d) Ca, and (e) Mg

4 To study the ratio of the residence time compared to the geochemical reaction time, we varied
5 the Darcy velocity (case study 3). The sensitivity of the simulated results has been tested by

1 increasing the Darcy velocity to 182 and 304 m years⁻¹ (case 3a (200 years), case 3b (100
2 years)) and decreasing it to 45 and 76 m years⁻¹ (case 3c (100 years), 3d (50 years)) for T1
3 and T2. The results of the third case study are shown in Figure 9.

4 As the results of case 3a and case 3b present the same spatial distribution of dissolved major
5 elements one may conclude that the residence time is not a key parameter of influence.
6 However, by comparing the results of cases 3c and 3d, especially in the case of transect T1,
7 there are significant differences between modelled concentrations of Na and Cl downstream
8 of zone 2. Furthermore, it is clearly shown that all modelled dissolved major elements exhibit
9 large differences in concentration when increasing (case 3b) or decreasing (case 3c) the
10 reference Darcy velocity by a factor of 2. This underlines that the modelled fate of dissolved
11 species is rather sensitive to the Darcy velocity. But the concentrations of the reference case
12 are located between these extreme cases.

13



- 1 **Figure 9:** Sensitivity study of the influence of the Darcy velocity (cases 3a, 3b, 3c and 3d)
- 2 on modelled dissolved major elements of the ground water: (a) Cl, (b) Na, (c) SO₄, (d) Ca,
- 3 and (e) Mg.

1 **4. Conclusions**

2 The Ouled Chamekh plain located in central-eastern Tunisia is a general example of a semi-
3 arid region where the problem of groundwater salinization is becoming more and more
4 severe. The shallow unconfined aquifer of Sidi El Hani is the main supply source of water.
5 Although a large amount of data has been obtained in previous studies, these studies did not
6 highlight the main factors responsible for the origin of the groundwater salinization in Sidi El
7 Hani. Therefore, further research was needed to identify the causes of groundwater
8 salinization at this site in a more integrated manner for application to the sustainable
9 management of groundwater resources.

10 The present study addresses the quantification and prediction of the chemical changes of
11 dissolved species in the groundwater, as well as the main geochemical processes that evolve
12 in the aquifer along a flow path. The rock-water interactions and mass transport along two
13 transects of the aquifer were simulated using the numerical hydrogeological code KIRMAT.
14 The calibrated reactive transport model underscores the observation along the two transects:
15 the concentrations of dissolved species such as chlorides, sodium, sulphates and calcium are
16 highly increased from the middle of each transect compared to the concentrations at the
17 inflow edge. However, in accordance with the field data, the calculated concentrations of
18 magnesium decrease along the flow path. These changes are clearly the result of the water-
19 rock interaction expressed by dissolution and precipitation. One may conclude that the
20 groundwater composition along the first 3 km of each transect is more specifically controlled
21 by the dissolution of halite, anhydrite, gypsum, calcite and dolomite. These processes are also
22 active in the remaining distance to the outflow edge of both transects, while gypsum changes
23 from under-saturated to over-saturated due to the accumulation of SO_4 ions. In addition, the
24 groundwater in these zones becomes saturated with respect to anhydrite. The results of the
25 modelled feedback effect of reactive mineral surfaces highlighted that the permeability of the
26 porous medium is globally increased.

27 The present study provides useful insights into the origin of salinization and the source of the
28 major elements in the groundwater in the Sidi El Hani basin: it specifies the origin of each
29 chemical element and the current state of its flux in the aquifer. The numerical studies using
30 the dynamic reactive transport model KIRMAT complete the actual knowledge of the
31 functioning of the aquifer and provide answers concerning the transport process involved.

32

1 **Acknowledgements**

2 The authors sincerely thank the CRDA of the Mahdia for giving free access to the plain. We
3 gratefully thank the farmers for their help during field work.

4 **References**

- 5 Ackerer, J., Chabaux, F., Lucas, Y., Clément, A., Fritz, B., Beaulieu, E., Viville, D., Pierret,
6 M.C., Gangloff, S., Négrel, Ph, 2018. Monitoring and reactive-transport modeling of the
7 spatial and temporal variations of the Strengbach spring hydrochemistry. *Geochim.*
8 *Cosmochim. Acta*, 225, 17-35.
- 9 APHA., 1995. Standard method for the examination of water and wastewater, 19th ed.
10 Washington, DC: American Public Health Association.
- 11 Appelo, J., Postma, D., 2005. *Geochemistry, groundwater and pollution*, 2nd ed. Balkema,
12 Rotterdam.
- 13 Appeli, C.A.J., Vinsot, A., Mettler, S., Wechner, S., 2008. Obtaining the porewater
14 composition of a clay rock modeling the in-and-out diffusion of anions and cations from
15 an in-situ experiment. *J. Contam. Hydrol.* 101, 67-76.
- 16 Alberto, W.D., Del Pilar, D.M., Valeria, A.M., Fabiana, P.S., Cecilia, H.A., De Los Angeles,
17 B.M., 2001. Pattern recognition techniques for the evaluation of spatial and temporal
18 variations in water quality. A case study: Suquia River Basin (Cordoba-Argentina). *Water*
19 *Res.* 35, 2881-2894.
- 20 André, L., Franceschi, M., Pouchan, P., Atteia, O., 2005. Using geochemical data and
21 modelling to enhance the understanding of groundwater flow in a regional deep aquifer,
22 Aquitaine Basin, south-west of France. *J. Hydrol.* 305, 40-62.
- 23 Belkhiri, L., Boudoukha, A., Mouni, L., Baouz, T., 2010. Application of multivariate
24 statistical methods and inverse geochemical modeling for characterisation of groundwater-
25 A case study : Ain Azel plain (Algeria). *Geoder.* 156 (3-4), 390-398.
- 26 Beig, M.S., Lüttge, A., 2006. Albite dissolution kinetics as a function of distance from
27 equilibrium: implications for natural feldspar weathering. *Geochim. Cosmochim. Acta.* 70
28 (6), 1402–1420.
- 29 Bel Hadj Salem, S., Chkir, N., Zouari, K., Cognard-Plancq, A.L., Valles. V., 2012.
30 Hydrochemical and isotope evidence of groundwater contamination of cultivated fields of
31 semi-arid environments in Tunisia. *Arid Land. Manage. J.* 26, 181-199.
- 32 Beaucaire, C., Michelot, J.J., Savoye, S., Cabrera, J., 2008. Groundwater characterisation and
33 modelling of water-rock interaction in an argillaceous formation (Tournemire, France).
34 *Appl. geochem.* 23, 2182-2197.
- 35 Bouchaou, L., Michelot, J.L., Vengosh, A., Hsissou, Y., Qurtobi, M., Gaye, C.B., Bullen,
36 T.D., Zuppi, G.M., 2008. Application of multiple isotopic and geochemical tracers for
37 investigation of recharge, salinization and residence time of water in the Souss-Massa
38 aquifer, southwest of Morocco. *J. Hydrol.* 352, 267-287.
- 39 Burch, T.E., Nagy, K.L., Lasaga, A.C., 1993. Free energy dependence of albite dissolution
40 kinetics at 80°C and pH 8.8. *Chem. Geol.* 105 (1–3), 137–162.

- 1 Colon, C.F.J., Oelkers, E.H., Schott, J., 2004. Experimental investigation of the effect of
2 dissolution on sandstone permeability, porosity, and reactive surface area. *Gochim.*
3 *Cosmochem. Acta.* 68, 805-817.
- 4 Daniele, L., Vallejos, A., Corbella, A., Molina, L., Pulido-Bosch, A., 2013.
5 Hydrogeochemistry and geochemical simulations to assess water-rock interactions in
6 complex carbonate aquifer: the case of aguadulce (SE Spain). *Appl. Geochem.* 29, 43-54.
- 7 Debye, P., Hückel, E. 1923. Zur Theorie der Elektrolyte. *Physics.* 24: 185-206.
- 8 De Montety, V., Radakovitch, O., Vallet-Coulomb, C., Blavoux, B., Hermitte, D., Valles, V.,
9 2008. Origin of groundwater salinity and hydrogeochemical processes in a confined
10 coastal aquifer. Case of the Rhone delta (Southern France). *Appl. Geochem.* 23, 2337-
11 2349.
- 12 Dridi, L., Majdoub, R., Hachicha, M., 2013. Modélisation hydrogéologique des écoulements
13 souterrains au niveau de la région d'OuledChamekh. Actes des 17^{ème} Journées
14 Scientifiques de l'INRGREF, Hammamet, Tunisie.
- 15 Droubi, A., Fritz, B., Tardy, Y. 1976. Equilibre entre minéraux et solutions : programmes de
16 calcul appliqués à la prédiction de la salure des sols et des doses optimales d'irrigation.
17 Cahier ORSTOM, série Pédologique. 10, 13-38.
- 18 Eissa, M.A., Thomas, J.M., Pohll, G., Shouakar-Stash, O., Hershey, R.L., Dawoud, M., 2016.
19 Groundwater recharge and salinization in the arid coastal plain aquifer of the Wadi Watir
20 delta, Sinai, Egypt. *Appl. Geochem.* 71, 48-62.
- 21 Eary, L.E., Runnells, D.D., Esposito, K.J. 2002. Geochemical controls on groundwater
22 composition at the Cripple Creek Mining District, Colorado. *Appl. Geochem.* 8(1), 1-24.
- 23 Edmunds, W.M., Shanda, P., Hartb, P., Wardc, R.S., 2003. The natural (baseline) quality of
24 groundwater: aUK pilot study. *Sci Total Environ.* 310, 25-35.
- 25 Edmunds, W.M., Carrillo-Rivera, J., Cardona, A., 2002. Geochemical evolution of
26 groundwater beneath Mexico City. *J. Hydrol.* 258, 1-24.
- 27 Essefi, H., Tourir, J., Tagorti, M.A., Yaich, Ch., 2014. Geodynamic framework of saline
28 systems in Eastern Tunisia: Saline Depressions inherited from the Triassic intrusion and/or
29 the Messinian Salinity Crisis. *ISRN Geol.* [Doi.org/10.1155/2014/798706](https://doi.org/10.1155/2014/798706).
- 30 Essefi, H., Tagorti., M.A., Tourir, J., Yachi, Ch., 2013. Hydrocarbons migration through
31 groundwater convergence towards saline depression. A case study Sidi El Hani, discharge
32 playa, Tunisian Sahel. *ISRN Environ. Chem.* [Doi.org/10.1155/2013/709190](https://doi.org/10.1155/2013/709190).
- 33 Farid, I., Zouari, K., Rigane, A., Beji, R., 2015. Origin of the groundwater salinity and
34 geochemical processes in detrial and carbonate aquifers: case of Chougafiya basin (Central
35 Tunisia). *J. hydrol.* 530, 508-532.
- 36 Gérard, F., 1996. Modélisation géochimique thermodynamique et cinétique avec prise en
37 compte des phénomènes de transport de masse en milieux poreux saturé. Thèse de
38 doctotrat. Université de Strasbourg. 250p.
- 39 Gérard, F., Clément, A., Fritz, B., Crovisier, J.L. 1996. Introduction des phénomènes de
40 transport dans le modèle thermo-cinétique KINDIS : le modèle KIRMAT. *C. R. Acad. Sci.*
41 *Parie*, tome 322, Série Iia, 377-384.

- 1 Gérard, F., Clément, F., Fritz, B., 1998. Numerical validation of an Eulerian hydrochemical
2 code using a 1-D multisolute mass transport system involving heterogeneous kinetically-
3 controlled reactions. *J. Contam. Hydrol.* 30(3-4), 199-214.
- 4 Gianbastiani, B.M.S., Colombani, N., Mastrocicco, M., Fidelibus, M.D., 2013.
5 Characterization of the lowland coastal aquifer of Comacchio (Ferrara, Italy): Hydrology,
6 hydrochemistry and evolution of the system. *J. Hydrol.* 501, 35-44.
- 7 Ghribi, R., Sghari, A., Bouaziz, S. 2008. Tectonic evolution of the oriental Tunisian platform
8 from miocene to quaternary," in *Proceedings of the 22nd Colloquium of African Geology*,
9 Hammamet, Tunisia.
- 10 Guo, Y.H., Shen, Z.L., Zhong, Z.S., 1997. The geochemistry simulation of groundwater
11 chemical environment evolution in Hebei plain. *Sci. China.* 27(4), 360-365.
- 12 Han, D.M., Song, X.F., Curell, M.J., Yang, J.L., Xiao, G.Q., 2014. Chemical and isotopic
13 constraints on evolution of groundwater salinization in the coastal plain aquifer of Laizhou
14 bay, China. *J. Hydrol.* 508, 12-27.
- 15 Helgeson, C.H. 1968. Evaluation of irreversible reactions in geochemical processes involving
16 minerals and aqueous solutions. I. Thermodynamic relations. *Geochim. Cosmochim. Acta.*
17 32, 853-877.
- 18 Jing, X., Yang, H., Wang, W., Cao, Y., 2016. Hydro-geochemical for the evolution of
19 groundwater quality in Yinchuan plain, China. *Hydrol. Sci. J.* 61(12),
20 <http://dx.doi.org/10.1080/02626667.2015.1111515>.
- 21 Kieffer, B., Jové, C.F., Oelkers, E.H., Schott, J. 1999. An experimental study of the reactive
22 surface area of the Fontainebleau sandstone as a function of porosity, permeability and
23 fluid flow rate. *Geochim. Cosmochim. Acta.* 63(21), 3525-3534.
- 24 Kim, K., 2002. Plagioclase weathering in the groundwater system of a sandy, silicate aquifer.
25 *Hydro. Processes* 16(9), 1793-1806.
- 26 Kumar, P.J., Elango, L., James, E.J., 2013. Assessment of hydrochemistry and groundwater
27 quality in the coastal area of South Chennai, India. *Arab. J. Geosci.* DOI [10.1007/s12517-](https://doi.org/10.1007/s12517-013-0940-3)
28 [013-0940-3](https://doi.org/10.1007/s12517-013-0940-3).
- 29 Lakshmanan, E., Kanan, R., Senthil, K.M. 2003. Major ion chemistry and identification of
30 hydro-geochemical processes of groundwater in a part of Kancheepuran district, Tamil
31 Nadu, India. *Envir. Geosci.* 10(4), 157-166.
- 32 Laabidi, E., Bouhlila, R., 2016. Reactive Henry problem: effect of calcite dissolution on
33 seawater intrusion. *Environ. Earth Sci. J.* 75(655), DOI: [10.1007/s12665-016-5487-7](https://doi.org/10.1007/s12665-016-5487-7).
- 34 Laabidi, E., Bouhlila, R., 2015. Nonstationary porosity evolution in mixing zone in coastal
35 carbonate aquifer using an alternative modeling approach. *Environ. Sci. Poll. Res.* 22,
36 10070-10082. DOI: [10.1007/s11356-015-4207-2](https://doi.org/10.1007/s11356-015-4207-2).
- 37 Li, P., Qian, H., Wu, J. 2014. Accelerate research on land creation. *Nature.* 7503 (510): 29-
38 31.
- 39 Li, P., Wu, J., Qian, H., 2013. Assessment of groundwater quality for irrigation purpose and
40 identification of hydro-geochemical evolution mechanisms in Pengyang County, China.
41 *Environ. Earth Sci.* 69(7), 2211-2225.
- 42 Li, P., Qian, H., Wu, J., Ding, J., 2010. Geochemical modeling of groundwater in southern
43 plain area of Pengyang County, Ningxia, China. *Water Sci. Eng.* 3(3), 282-291.

- 1 Li, Y.L., Wang, Y.X., Zhou, L.R., 2002. Hydro-geochemical modeling on saturation of
2 minerals in groundwater. A case study at Niangzigun, Northern China. *Geol. Sci.Tech. Inf.*
3 21(1), 32-36.
- 4 Lopez-Chicano, M., Ouamama, M., Vallejos, A., Pulido-Bosch, A., 2001. Factors which
5 determinate the hydrogeochemistry behavior of karstic springs: a case study from the
6 Betic Cordilleras, Spain. *Appl. Geochem.* 16, 1179-1192.
- 7 Lucas, Y., Schmitt, A.D., Clement, A., Ftriz, B., Elsass, Ph., Durand, S., 2010. Geochemical
8 tracing and hydrogeochemical modeling of water-rock interaction during salinization of
9 alluvial groundwater (Upper Rhine Valley, France). *Appl. Geochem.* 25, 1644-1663.
- 10 Lucas, Y., Chabaux, F., Schaffhauser, T., Fritz, B., Ambroise, B., Ackerer, J., Clément, A.
11 (2017). Hydrogeochemical modeling (KIRMAT) of spring and deep borehole water
12 compositions in the small granitic Ringelbach catchment (Vosges Mountains, France).
13 *App. Geochem. J.* 87, 1-21.
- 14 Madé, B., Clément, A., Fritz, B., 1994. Modelling mineral/solution interactions: The
15 thermodynamic and kinetic code KINDIS. *Comput. Geosci.* 20(9), 1347-1363.
- 16 Maher, K., Steefel, C.I., DePaolo, D.J., Viani, B.E., 2006. The mineral dissolution rate
17 conundrum: Insights from reactive transport modeling of U isotopes using U isotopes and
18 pore fluid chemistry in marine sediments. *Geoch. et Cosmochem. Acta*, 70, 337-363.
- 19 M'nassri, S., Dridi, L., El Amri, A., Hachicha, M., Majdoub, R. 2016. Aptitude des eaux de
20 la nappe phréatique de la cuvette de Sidi El Hani à l'irrigation (Centre-East, Tunisie). *J.*
21 *Mater. Environ. Sci.* 7(12), 4742-4753.
- 22 M'nassri, S., Dridi, L., Lucas, Y., Schäfer, G., Hachicha, M., Majdoub, R. (2018). Identifying
23 the origin of groundwater salinisation in the Sidi El Hani basin in central-eastern, Tunisia.
24 *J. Afr. Earth Sci.* 147, 443-449.
- 25 Majdoub, R., Hachicha, M., El Amri, A., Melki, M. 2012. Etude de la dynamique de l'eau et
26 du transfert des sels dans un sol sablo-limoneux du sahel Tunisien. *Euro. J. Sci. Res.*
27 80(4), 499-507.
- 28 Marty, N.C., Ftriz, B., Clément, A., Michau, N., 2010. Modeling the long term alteration of
29 the engineered bentonite barrier in an underground radioactive waste repository. *Appl.*
30 *Clay Sci.* 47(1-2), 82-90.
- 31 Marty, N.C., Tournassat, C., Brunol, A., Giffaut, E., Gaucher, E., 2009. Influence of reaction
32 kinetics and mesh refinement on the numerical modelling of concrete/clay interactions. *J.*
33 *hydrol.* 364, 58-72.
- 34 Marty, N., 2006. Modélisation couplée (transport-réaction) des interactions fluids-argiles et
35 de leurs effets en retour sur les propriétés physiques de barrières ouvragées en bentonite.
36 Thèse de doctorat. Université de Strasbourg. 314p.
- 37 Merdith, K., Cendon, D.I., Pigois, J.P., Hollins, S., Jacobsn, G., 2012. Using ¹⁴C and ³H to
38 delineate a recharge window into the Perth Basin aquifer, North Gngangara groundwater
39 system. Western Australia. *Sci. Tot envir.* 414, 456-469.
- 40 Meunier, A., 2006. Why are the clay minerals small? *Clay Min.* 41(2), 551-566.
- 41 Milnes, E., 2011. Process-based groundwater salinisation risk assessment methodology:
42 Application to the Akrotiri aquifer (Southern Cyprus). *Hydrol. J.* 399, 29-47.

- 1 Molins, S., Trebotich, D., Steefel, C.I., Shen, C., 2012. An investigation of the effect of pore
2 scale flow on average geochemical reaction rates using direct numerical simulation. *Water*
3 *Resour. Res.* 48(3). Doi:10.1029/2011WR011404.
- 4 Montes, G.H., Fritz, B., Clément, A., Michau, N., 2005a. A simplified method to evaluate the
5 swelling capacity evolution of a bentonite barrier related to geochemical transformations.
6 *Appl. Geochem.* 20, 409-422.
- 7 Montes, H.G., Fritz, B., Clement, A., Michau, N. 2005b. Modeling of transport and reaction
8 in an engineered barrier for radioactive waste confinement. *Appl. Clay Sci.* 29 (3-4), 155-
9 171.
- 10 Montcoudiol, N., Molson, J., Lemieux, J.-M., Cloutier, V. 2015. A Conceptual model for
11 groundwater flow and geochemical evolution in the southern Outaouais region, Québec
12 Region, Québec, Canada. *Appl. Geochem.* 58, 62-77.
- 13 Najib, S., Fadili, A., Mehdi, K., Riss, J., Makan, A., Guessir, H., 2016. Salinization process
14 and coastal groundwater in Chaouia, Morocco. *J. Afr. Earth Sci.* 115, 17-31.
- 15 Nasri, N., Bouhlila, R., Maarten, W., Pablo, G., 2016. Modeling the hydrogeochemical
16 evolution of brine in saline systems: Case study of the sabkha of Oum El Khialate in South
17 East Tunisia. *Appl. Geochem.* 55, 160-1693.
- 18 Nield, D.A., Simmons, T.C., Kuznetsov, A.V., Ward, J.D. 2008. On the evolution of salts
19 lakes: Episodic convection beneath an evaporating salt lake. *Water Resour. Res.* 44(2),
20 DOI: 10.1029/2007WR006161.
- 21 Ngo, V.V., Lucas, Y., Clément, A., Fritz, B. 2016. Modeling the impact of temperature on the
22 saturation state and behavior of minerals in the Soultz-sous-Forêts geothermal system.
23 *Geother.* 64, 196-208.
- 24 Ngo, V., Delalande, M., Clement. A., Michau, N., Fritz, B. 2014. Coupled transport-reaction
25 modelinf of the long-term interaction between iron, bentonite and Callovo-Oxfordian
26 claystone in radioactive confinement systems. *Appl. Clay Sci.* 101, 430-443.
- 27 Nouertier-Mazauric, E., Guy, B., Fritz, B., Brosse, E., Gracia, D., Clément, A., 2005.
28 Modelling the dissolution/precipitation of ideal solid solution. *Oil Gas Sci. technol. Rev.*
29 *IFP*, 60(2): 401-415.
- 30 Nourtier-Mazauric, E., 2006. Modélisation géochimique et numérique des interactions entre
31 des solutions solides et une solution aqueuse. Extension du logiciel de réaction-transport
32 Archimède et application à la diagenèse minérale des réservoirs. Thèse de doctorat. Ecole
33 nationale supérieure des mines de Saint-Etienne et de l'université de Jean Monnet. 218p.
- 34 Pacheco, F., Van der Weijden C., 2014. Modeling rock weathering in small watersheds. *J.*
35 *hydrol.* 513, 13-27.
- 36 Palandari, J., Kharaka, Y.K., 2004. A compilation of rate parameters of water-mineral
37 kinetics for application to geochemical modeling (No. Open-File-2004-1068) Geological
38 Survey Menlo Parck CA.
- 39 Peikam, N., Jalali, M., 2015. Application of inverse geochemical modeling for predicting
40 surface water chemistry in Ekbatan watershed, Hamedan, Western Iran. *Hydrol. Sci. J.*
41 <http://dx.doi.org/10.1080/02626667.2015.1016947>.
- 42 Prikryl, D., Jha, A., Stefansson, S., Stipp, S.L. 2017. Mineral dissolution in porous media: An
43 experimental and modeling study kinetics, porosity and surface area evolution. *Appl.*
44 *Geochem. J.* 87, 57-70.

- 1 Rajmohan, N., Elango, E.L., 2004. Identification and evolution of hydrogeochemical processes
2 in the groundwater environment in area the Palar and Cheyyar River Basins, Southern
3 India. *Environ. Geol. J.* 46, 47-61.
- 4 Sikdar, P.K., Sarkar, S.S., Palchoudhury, S., 2001. Geochemical evolution of groundwater in
5 the Quaternary aquifer of Calcutta and Howrah, India. *J. Asi. Earth Sci.* 19, 579-594.
- 6 Sparks, L.D., 2003. Ion exchange processes. *Environ. Soil. Chem.* (2 edition). 187-205.
- 7 Steefel, C.I., Appelo, C.A.J., Arora, B., Jacques, D., Kalbacher, T., Kolditz, O., Lagneau, V.,
8 Lichtner, P.C., Mayer, K.U., Meeussen, J.C.L., Molins, S., 2015. Reactive transport codes
9 for subsurface environmental simulation. *Computat. Geosci.* 19(3), 445-478.
- 10 Tagorti, M.A., Essefi, H., Touir, J., Guellala, R., Yaich Ch., 2013. Geochemical controls of
11 groundwater upwelling in saline environments : Case study the discharge playa of Sidi El
12 Hani (Sahel, Tunisia). *Afr. Earth Sci. J.* 86, 1-9.
- 13 Wu, P., Tang, C., Zhu, L., Liu, C., Cha, X., Tao, X., 2009. Hydrogeochemical characteristics
14 of surface water and groundwater in the karst basin, southwest China. *Hydrol. processes.*
15 23, 2012-2022.
- 16 Wilson, J.C., Benbow, S., Watson, C., Sasamoto, H., Savage, D. 2015. Thermodynamic and
17 fully-coupled reactive transport models of a steel-bentonite interface. *Appl. Geochem.* 61,
18 10-28.
- 19 White, A.F., Brantley, S.L, 2003. The effect of time on the weathering of silicate minerals:
20 Why do weathering rates differ in the laboratory and field? *Chem.Geol.* 202 (3-4), 479-
21 506.
- 22 Xiao, J., Zhang, J., Zhang, F., Wang, J., 2012. Solute geochemistry and its sources of the
23 groundwaters in the Qinghai Lake catchment, NW china. *J. Asi Earth Sci.* 52: 21-30.

24

25

26